NEW VIEW OF THE MARTIAN SURFACE: THEMIS GLOBAL THERMAL INERTIA MOSAIC. R. L. Fergason[1] and P. R. Christensen[2], [1]United States Geologic Survey, 2255 N. Gemini Dr., Flagstaff, AZ 86001, rfergason@usgs.gov, [2]Mars Space Flight Facility, Arizona State University, PO Box 876305, Tempe, AZ 85287-6305.

Introduction: Thermal inertia derived from Thermal Emission Spectrometer (TES) data at 20-ppd [1-2] is the highest spatial resolution global thermal inertia dataset currently available. This valuable dataset is important for understanding regional variations in thermal inertia, and for inferring the physical nature of the surface at 10s to 100s of km scales. However, the resolution of TES (~3 km per pixel) is a major limitation, as this spatial resolution is often not sufficient to infer the physical properties of, or relative differences between, morphologic features observed in high-resolution images, including Mars Orbiter Camera (MOC) [3], Thermal Emission Imaging System (THEMIS) [4], and High Resolution Imaging Science Experiment (HiRISE) [5] or to understand geologic processes acting on local scales. Many features that have important implications for the geologic and climactic history of Mars, including exposed bedrock or layered deposits, are too small to be uniquely identified in TES data.

In this study, we are generating a new global thermal inertia mosaic using high resolution THEMIS data. The THEMIS instrument onboard Mars Odyssey is obtaining infrared observations of the martian surface at the highest spatial resolution to date (100 m per pixel) [4]. These data are currently used to calculate thermal inertia values of local regions (100-m scales) and to improve the interpretation of particle size distributions and material properties of local surfaces observed in high-resolution visible images [e.g. 6-12]. This new mosaic has facilitated an improved understanding of the nature of moderate thermal inertia surfaces. Specifically indurated material may be the primary cause of moderate thermal inertia surfaces. Features such as aeolian derived sediment, rocky material, crater ejecta, exposed ridges, cliffs, and crater rims all act to further increase the thermal inertia in the local regions where they are present, but these features alone do not explain the moderate thermal inertia values observed.

Method: We are creating a global thermal inertia mosaic in 30° latitude by 30° longitude bins, resulting in 48 individual thermal inertia mosaics (Figure 1). These mosaics will then be pieced together to complete a global thermal inertia mosaic between ±60° latitude at a spatial resolution of 256 ppd (equivalent to ~230 m per pixel at the equator). The 48 individual mosaics and the global mosaic, in both image (e.g. png, tiff, and jpeg) and data (e.g. vicar) formats, will be made available to the community through the Planetary Data System (PDS).

To generate this mosaic, thermal inertia values are first derived from individual THEMIS nighttime infrared images using the technique of *Fergason et al.* [10]. The brightness temperature of the surface is determined by fitting a Planck curve to band 9 (centered at 12.57 μm) calibrated radiance that has been corrected for instrumental effects [4]. The THEMIS band 9 temperatures are converted to a thermal inertia by interpolation within a 7-dimensional look-up table using latitude, season, local solar time, atmospheric dust opacity, thermal inertia, elevation (atmospheric pressure), and albedo as input parameters. Season, latitude, and local solar time are determined from spacecraft ephemeris. The remaining model input parameters (albedo, elevation, and atmospheric dust opacity) are obtained from external datasets. The absolute accuracy of the THEMIS thermal inertia is ~20%. Uncertainties in the THEMIS derived thermal inertia values are primarily due to: 1) instrument calibration; 2) uncertainties in model input parameters at the resolution of the THEMIS instrument; and 3) thermal model uncertainties [10].

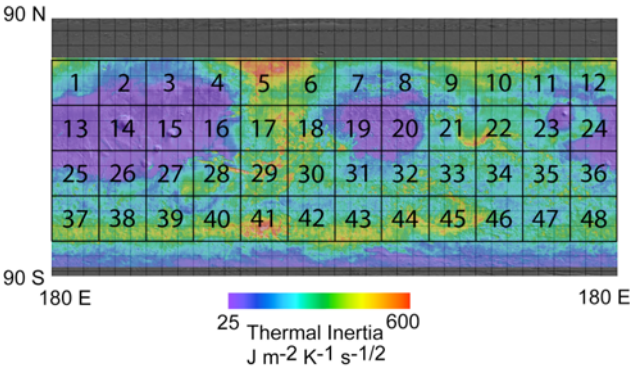

Figure 1. THEMIS global thermal inertia mosaic. 30° latitude by 30° longitude bins are being created, resulting in 48 individual thermal inertia mosaics. These mosaics are then pieced together to complete a global thermal inertia mosaic between ±60° latitude.

Once thermal inertia is derived from individual THEMIS images, these images are projected into a simple cylindrical projection using ISIS geometry software [13]. Images between ±60° latitude are then mosaicked together, using software similar to that developed to make THEMIS daytime and nighttime temperature mosaics [14]. To maximize the quantitative nature of the information present in the mosaic, no normalization or blending is used in the mosaicking process. Thermal inertia is independent of season and local time, and thus image-to-image differences are typically less apparent in thermal inertia than temperature data. However, image-to-image differences can still be prominent in derived thermal inertia. Some of the variations between images are due to uncertainties in the input parameters and in the thermal models, but the majority of discrepancies are likely due to uncertainties in the calibration of the THEMIS instrument. Much of this uncertainty is present because THEMIS calibration requires an image of a calibration flag that is typically acquired 60-90 seconds after the end of each THEMIS IR image. During this 60-90 second gap, instrument conditions can change slightly, including slight changes in the temperature of the focal plane array. This causes a radiance offset of the entire image that results in a random (between images) error with a standard deviation of ~4 K at 180 K [10].

The uncertainty in the THEMIS calibration is reduced by comparing the measured atmospheric radiance between THEMIS (band 10, centered at 14.88 μm) and TES.

The radiometric accuracy of TES is better than THEMIS (~1 to 2 K at 180 K [4, 15]) and, outside periods of high dust activity, martian atmospheric properties are quite repeatable from year to year [16-17]. By binning TES data as a function of location and season (MGS and M01 local time differences in measured radiance intergrated over band 10 are not significant) and convolving it to THEMIS band 10 radiance, it is possible to predict the THEMIS measured radiance. Any difference between the TES predicted and THEMIS measured band 10 radiance is assumed to be due to calibration error and is converted to a raw DN equivalent radiance correction for each of the THEMIS channels. We avoid periods of high dust opacity (9 micron opacities >0.30) present in either the THEMIS or TES datasets because of the inherent variability in the martian atmosphere present during these periods. Application of this technique has reduced image-to-image variations in THEMIS data.

Results and Discussion: The global-scale derivation of thermal inertia at a spatial scale applicable to high-resolution visible images enables a more complete understanding of the surface properties of Mars. Broad regions of low thermal inertia (< 120 $Jm^{-2}K^{-1}s^{-1/2}$) in the Tharsis Montes, Arabia Terra and Elysium Mons regions have been interpreted as a mantle of air-fall dust up to ~1 m in thickness [e.g. 18-19, 1, 10]. High inertia (>600 $Jm^{-2}K^{-1}s^{-1/2}$) surfaces primarily observed in the outflow channels and Valles Marineris, southern Isidis Planitia, and the rim of Hellas basin have been interpreted as having exposures of bedrock or very rocky materials [e.g. 20-21, 2, 7]. However, surfaces with a moderate thermal inertia (~120 to ~600 $Jm^{-2}K^{-1}s^{-1/2}$) are more difficult to interpret because intermediate thermal inertia values can be caused by many different combinations of particle size mixtures, layered materials, and degree of induration [e.g. 1-2, 10]. Although the interpretation of intermediate thermal inertia values is ambiguous, this surface type represents a majority of the martian surface, and it is therefore important to constrain the possible formation mechanisms. There are four likely origins of intermediate thermal inertia materials: 1) unconsolidated, aeolian derived sediment; 2) indurated material; 3) thin layers of fine unconsolidated material (often dust) overlying coarser materials, such as rocky surfaces or exposed bedrock; and 4) sub-pixel mixing of particle sizes. The sub-pixel mixing of materials cannot be positively identified, but the remaining processes can be inferred from morphologic features, albedo, and topographic controls.

In the analysis of 12 locations on Mars containing moderate thermal inertia materials, all locations likely have a significant amount of indurated material. Features such as aeolian derived sediment, rocky material, crater ejecta, exposed ridges, cliffs, and crater rims all act to further increase the thermal inertia in local areas where they are present, but these features alone do not explain the regional thermal inertia values observed. In surfaces with a thermal inertia greater than 400 $Jm^{-2}K^{-1}s^{-1/2}$ indurated material alone cannot explain the high thermal inertia values [22], and rocky material or exposed bedrock is likely more prevalent in these locations. Therefore, indurated material may be the primary cause of moderate thermal inertia surfaces, and is very likely present over the majority of martian surfaces. This result helps to confirm previous suggestions using Viking and TES data [e.g. 23, 1-2, but the combination of higher-resolution thermal inertia data from THEMIS and high-resolution visible images (e.g. MOC, THEMIS VIS, and HiRISE) enables confirmation and improved characterization of this hypothesis.

Soils analyzed at the VL1 [24] and Spirit [25] landing sites indicate that indurated material contains sulfates, and presumably these salts act as the cementing agent. This process is likely facilitated by the presence of water. Subsurface aquifers, standing bodies of water, the condensation of atmospheric water vapor, and the condensation and subsequent sublimation of subsurface water-ice are all possible mechanisms for the cementation of soils. The process(s) by which this globally-pervasive duricrust formed, and the variations in both the physical characteristics of the duricrust and the potential formation mechanism, is critical for understanding the past role of water on Mars and the martian climate history. Future work will include assessing additional regions of moderate thermal inertia to determine the global variation of surface properties of this surface type, and to utilize regional morphology and geologic context to constrain possible cementation mechanisms at each location. From this work, an improved understanding of the variation in the physical properties of moderate thermal inertia surfaces present on Mars and the geologic processes that produced these variations will result.

References:

[1] Mellon, M. T. et al. (2000) *Icarus, 148*, 437-455. [2] Putzig, N. E. et al. (2005) *Icarus, 173*, 325-341. [3] Malin, M. C. and Edgett, K. S. (2001) *JGR, 106*, 23,429-23,570. [4] Christensen, P. R. et al. (2004) *Space Sci. Rev., 110*, 85-130. [5] McEwen, A. S. et al. (2007) *JGR, 112*, doi:10.1029/2005JE002605. [6] Christensen, P. R. et al. (2003) *Science, 300*, 2056-2061. [7] Christensen, P. R. et al. (2005) *Nature*, 436, doi:10.1038/nature03639. [8] Rogers, A. D. et al. (2005) *JGR, 110*, doi:10.1029/2005JE002399. [9] Fenton, L. K. and Mellon, M. T. (2006) *JGR, 111*, doi:10.1029/2004JE002363. [10] Fergason, R. L. et al. (2006) *JGR, 111*, doi:10.1029/2006JE002735. [11] Michalski, J. R. and Fergason, R. L. (2008) *Icarus, 199*, 25-48. [12] Fergason, R. L. and Christensen, P. R. (2008) *JGR, 113*, doi:10.1029/2007JE002973. [13] Eliason, E. M. (1997), *Lunar Planet. Sci. XXVIII*, 17-21. [14] Gorelick, N. S. and Christensen, P. R. (2005), *Eos Trans.AGU, 86*, Abstract P21C-0161. [15] Christensen, P. R. et al. (2001) *JGR, 106*(E10), 23,823-23,871. [16] Clancy, R. T. et al. (2000) *JGR, 105*, 9553-9571. [17] Smith, M. D. (2004) *Icarus, 167*, 148-165. [18] Kieffer, H. H. et al. (1977) *JGR, 82*, 4249-4291. [19] Palluconi, F. D. and Kieffer, H. H. (1981) *Icarus, 45*, 415-426. [20] Christensen, P. R. and Kieffer, H. H. (1979) *JGR, 84*, 8233-8238. [21] Pelkey, S. M. and Jakosky, B. M. (2002) *Icarus, 160*, 228-257. [22] Nowicki, S. A. and Christensen, P. R. (2007) *JGR, 112*, doi:10.1029/2006JE002798. [23] Jakosky, B. M. and Christensen, P. R. (1986) *JGR, 91*, 3547-3559. [24] Clark, B. C. and Van Hart, D. C. (1981) *Icarus, 45*, 370-378. [25] Yen, A. S. et al. (2005) *Nature, 436*, doi:10.1038/nature03637.